Volume 1 | Number 1 | Jan 2013 | Pages 1–100

Nanoscale

www.rsc.org/nanoscale

ROYAL SOCIETY OF CHEMISTRY

This is an *Accepted Manuscript*, which has been through the Royal Society of Chemistry peer review process and has been accepted for publication.

Accepted Manuscripts are published online shortly after acceptance, before technical editing, formatting and proof reading. Using this free service, authors can make their results available to the community, in citable form, before we publish the edited article. We will replace this *Accepted Manuscript* with the edited and formatted *Advance Article* as soon as it is available.

You can find more information about *Accepted Manuscripts* in the **Information for Authors**.

Please note that technical editing may introduce minor changes to the text and/or graphics, which may alter content. The journal's standard **Terms & Conditions** and the **Ethical guidelines** still apply. In no event shall the Royal Society of Chemistry be held responsible for any errors or omissions in this *Accepted Manuscript* or any consequences arising from the use of any information it contains.

www.rsc.org/nanoscale

Journal Name

Nanoscale

ARTICLE TYPE

In situ synthesis of luminescent carbon nanoparticles toward target bioiomaging

Shazid Md. Sharker[a] , **Sung Min Kim**[b], **Jung Eun Lee**[c], **Ji Hoon Jeong**[c], **Insik In**[d, e], **Kang Dea Lee**[f], **Haeshin Lee** [a*] **and Sung Young Park**[b, e]*

This paper describes *in situ* synthesis of single fluorescence carbon nanoparticle (FCN) for target bioimaging application derived from biocompatible hyaluronic acid (HA) without using common conjugation process. The FCN formed *via* dehydration of hyaluronic acid which was completed carbonized HA, and partial carbonized HA (HA-FCN) formed by the degree of carbonization process shows good 10 aqueous solubility, small particle size (<20 nm) and different fluorescence intensity with a red shift. After the confirmation of the cytotoxicity of HA-FCN and FCN, we carried out *in vitro* and *in vivo* bioimaging studied where the HA-FCN itself appeared single particle trigger targeted imaging for the probe. The converted nanocrystal carbon particle by HA allowed biological potentiality for *in vitro* and *in vivo* system that speculates outstanding features for generating new target delivery and diagnostic tools.

Introduction

15 The profound application of fluorescent carbon nanoparticles (FCNs) has generated an extended demand to acquire next generation FCN. However, in respect to biocompatibility, bio stability and scope of further fabrication, the currently available FCNs are still struggling to maintain integrity, sensitivity and 20 selectivity.[1] In general, it is believed that the identical features of a bio-composite are greatly dependent on size, shape and elemental composition; changes of any of these can significantly modify the native features.[2]

Since the discovery of Hyaluronic Acid (HA), one of the main 25 components of body tissues, it has been used alone or in conjugation with other materials in different fields of life science.[3, 4] The biodegradable repeated disaccharide polymer of HA was found to retain unique viscoelasticity, limited immunogenicity, and is easily chemically cross-linked with other 30 components. The poly-disaccharide HA polymers also found predominantly in the extracellular matrix (ECM) of connective tissues, and plays important roles in organization of the ECM, as well as cell motility, adhesion, and differentiation. However, in uncontrolled growing non-differentiated tumor angiogenesis, the 35 CD44 receptor, which binds HA ligand, is also found abundantly.[3] These properties have made HA one of the leading bio-composites.[5] The recent status of the HA-fabricated drug delivery system (DDS), tissue engineering, and the innovative biomaterial designed have fascinated the scientific community.[6] 40 In the field of bio-sensing, FCN shows unique chemical and optical properties over the traditional fluorescence organic probe.[7] The use of fluorescent nanoparticles based on semiconductors, metal, silica, polymers, etc., have been a major focus during the past decades, to develop more effective

45 biosensors and bio-levelling imaging probes. Their sensitivity, stability and capability of multiplexing make them one of the most useful tools enabling intracellular monitoring for biomedical and biological purposes.[1] However, the size, shape and concentration-dependent cytotoxic effects, as well as 50 physiological hepatotoxicity, have been considered the major drawbacks.[8, 9] Moreover, there is still little diversity in FCN materials available, and most of them are in the development stage. The huge biochemical and biomedical field is always seeking the most promising FCN, possessing advanced sensitivity 55 and selectivity.[10]

Most notable, the potential replacement for toxic metal-based quantum dots (QDs) and inspired by the electronic response of carbon dots (C-dots), in which size, shape and composition can all be tailored to create a variety of desired properties, we 60 attempted to fabricate a bio-composite (HA), capable of absorbing and emitting light in a defined wavelength.[11, 12] Herein, we developed a hyaluronic acid fluorescent carbon nanoparticle (HA-FCN) and a fluorescent carbon nanoparticle (FCN) from hyaluronic acid (HA). In detail, water-dissolved HA was 65 carbonized in a defined dehydrating agent at a control temperature, and depending on the reaction time, HA-FCN and FCN were obtained separately. At the end of the process, the resulting product was neutralized using alkali solution, followed by dialysis to obtain the purified products.

70

Experimental Section
Materials

Trizma base, Trizma HCl, [3-(4,5-dimethylthiazol-2-yl)-2,5-diphenyltetrazolium bromide] (MTT), Triton X-100, concentrated 75 H_2SO_4 and H_3PO_4 were purchased from Sigma Aldrich, Korea. Hyaluronic acid (Mw 2,000 kDa) was obtained from Shinpoong

Pharm, (Korea) as a kind donation. Penicillin-streptomycin, fetal bovine serum (FBS), 0.25% (w/v) Trypsin, 0.03% (w/v) EDTA solution, and RPMI-1640 medium were purchased from Gibco BRL (Carlsbad, A, USA).

[5] ^{1}H NMR spectra were recorded on a Bruker Advance 400 MHz spectrometer using deuterium oxide (D$_2$O) as the solvent. The X-ray diffraction (XRD; Bruker AXS ADVANCE D-8), and UV–vis spectra were recorded using an Optizen 2020UV. Particle size was measured using dynamic laser light scattering (Zetasizer [10] Nano, Malvern-Germany). Transmission Electron Microscopy (FEI, Netherlands) and XPS results were obtained using an Omicrometer ESCALAB (Omicrometer, Taunusstein, Germany). AFM imaging was carried out in tapping mode on a MultiMode8 (Bruker) with a silicon probe. For AFM images, samples were [15] prepared on silicon wafers. Thermal gravity analysis (TGA) was performed by a TGA-DSC1 system (Star; Mettler Toledo). Photoluminescence (PL) spectra were obtained from a L550B luminescence spectrometer from Perkin Elmer. Fluorescence lifetimes were measured using a NanoLED laser light source [20] (Horiba Jobin Yvon NanoLog spectrophotometer) at 375 nm for the excitation, and the data were fitted by a multi-exponential decay model. The samples for the fluorescence lifetimes measurements were prepared by dissolving HA-FCN and FCN in an aqueous solution at very low concentrations (1.0 mg mL^{-1}). [25] Elemental analyses were performed by using an EA1110 Fisons analyzer. Dynamic light scattering (DLS) data were obtained using a particle size analyzer (ELS-Z) from Otsuka Electronics Corporation. The molecular weights of HA-FCN and FCN were measured using gel permeation chromatography (GPC). The GPC [30] measurements were performed on a Waters 2410 with an RI (Refractive Index) detector and 0.1M NaCl in H$_2$O as the eluent. The following separation columns were installed in the GPC: Shodex SB-802 HQ (Exclusion Limit 4,000); SB-803 HQ (exclusion limit 100,000); SB-804 HQ (exclusion limit [35] 1,000,000); SB-805 HQ (exclusion limit 4,000,000). Quinine sulphate (QY 55 (%) at 354 nm excitation) was used as a reference standard to measure quantum yield, as adapted from a published report elsewhere.[13] Raman spectra were investigated using a Laser Raman spectrophotometer (NRS-3200 Jasco, [40] Japan).

HA-FCN and FCN synthesis

The synthesis method was adopted from a similar report in the literature.[14] In a typical procedure, Hyaluronic Acid Fluorescent Carbon Nanoparticle (HA-FCN) was synthesized by dissolving [45] 0.20 g of Hyaluronic Acid (HA) in water and mixing with 10 mL H$_2$SO$_4$ (30N) for about 1.5 minutes, after which 75 mL of NaOH (4 N) was added to neutralized the acid. Dialysis (molecular weight cutoff of 3500) against water was carried out for purification, and finally freeze-dried to obtain the products (85% [50] yields).

In the same way, Fluorescent Carbon Nanoparticle (FCN) was obtained by dissolving 0.25 g of Hyaluronic Acid (HA) in water and mixing with 10 mL H$_2$SO$_4$ (30 N) for about 10 minutes, after which 75 mL of NaOH (4 N) was used to neutralized the H$_2$SO$_4$. [55] Dialysis was performed (molecular weight cutoff of 3500) against water for purification, followed by freeze-drying to obtain the desired products (18% yields). However, the reaction conditions needed to be finely adjusted to minimize particle aggregation. All synthesis was carried out at room temperature.

[60] ### Cytotoxicity assay

The cytotoxicity was measured using the [3-(4, 5-dimethylthiazol-2-yl)-2, 5-diphenyltetrazolium bromide] MTT assay method. In brief, 200 μL of cells, at a density of 2×10^5 cells mL^{-1}, were placed in each well of a 96-well plate. The cells were then incubated for 24 hours at 37 ℃ in a humidified 5% [65] CO$_2$ atmosphere. To determine cell viability, a stock solution of HA-FCN and FCN was dissolved in RPMI medium at the concentration of 1 mg mL^{-1}, and the stock solution was then diluted up to 0.01 mg mL^{-1}. The media was removed, and the [70] cells were treated with the different prepared concentrations of HA-FCN and FCN, respectively. The cells were further incubated for another 24 hours as was done previously. The media containing the drug was then replaced with 180 μL of fresh medium and 20 μL of a stock solution containing 15 mg of MTT [75] in 3 mL PBS, after which the cells were incubated for another 4 h. Finally, the medium was removed and 200 μL of MTT solubulizing agents were added to the cells. Mild shaking was performed for 15 min, and the absorbance was measured at 570 nm using a microplate reader (Varioskan Flash, Thermo [80] Electron Corporation). The relative cell viability was measured by comparison with the control 96-well, containing only cells.

In vitro cell imaging

The HA-FCN and FCN incubated cells were analyzed by confocal imaging. The MDAMB-231, A549 and MDCK cells [85] were plated over a cover slide on an eight-well plate at a density of 2×10^5 cells mL^{-1} per well, and were incubated for 24 hours at 37 °C in a humidified 5% CO$_2$ atmosphere. The cells were treated with the fluorescent nano-particles (HA-FCN and FCN) at concentrations of 0.01 mg mL^{-1} for 2 h in fresh culture media. [90] The media were then washed with PBS several times to remove the unbound composite materials. Finally, the cells were examined using an LSM510 confocal laser scanning microscope (Carl Zeiss, Germany). An excitation wavelength of 488 nm was used, with an emission filter of 505 nm. During all investigations, [95] the objective lens was kept at 20X.

Evaluation of cellular uptake

To quantify the cellular uptake of HA-FCN and FCN, cancerous MDAMB-231 and normal MDCK cells were selected and seeded in a 12-well plate at a concentration of 0.5×10^5 cells mL^{-1}.[15] [100] After 24 hours of incubation, the media were removed, and the cells were treated with 0.5 mg/mL of HA-FCN or FCN containing media. Cells were then allowed to incubate for another 4 hours. At the end of the period, the sample containing media was removed, and the cells were washed several times with PBS [105] (1X, pH 7.4). Triton X-100 (1%) was then used to lyse the cells. The relative amounts of accumulated HA-FCN and FCN within the cell interior were determined by measuring the fluorescence intensity at excitation wavelengths of 340 nm and 380 nm, respectively, with a microplate fluorescence spectrophotometer [110] reader (Varioskan Flash, Thermo).

In vivo bioimaging and biodistribution

Balb/c mouse were properly cared for, and were considered for experimental investigation at the age of six weeks. All animal studies were approved by the SKKU School of Pharmacy [115] Institutional Animal Care Committee. To observe biodistribution of the HA-FCN and FCN separately in an animal model, the athymic nude mice (4.5-week old, 20-25 g, male) were prepared by inoculating a suspension of 1x10^7 MDAMB-231 cells in saline (60 μL) into left flanks of mice. When tumors grew to [120] approximately 250-500 mm^3 in volume, 200 μL of PBS containing HA-FCN or FCN (30 mg kg^{-1}) were injected into the tail vein (n=3 per each group). They were then sacrificed at 24 hrs post injection, and the major organs were excised and observed by the Kodak image station (Kodak Image Station [125] 4000MM, New Haven, CT, USA). All near infrared fluorescence (NIRF) intensities were calculated using the Analysis Workstation software (ART Advance Research Technologies Inc., Montreal, Canada).
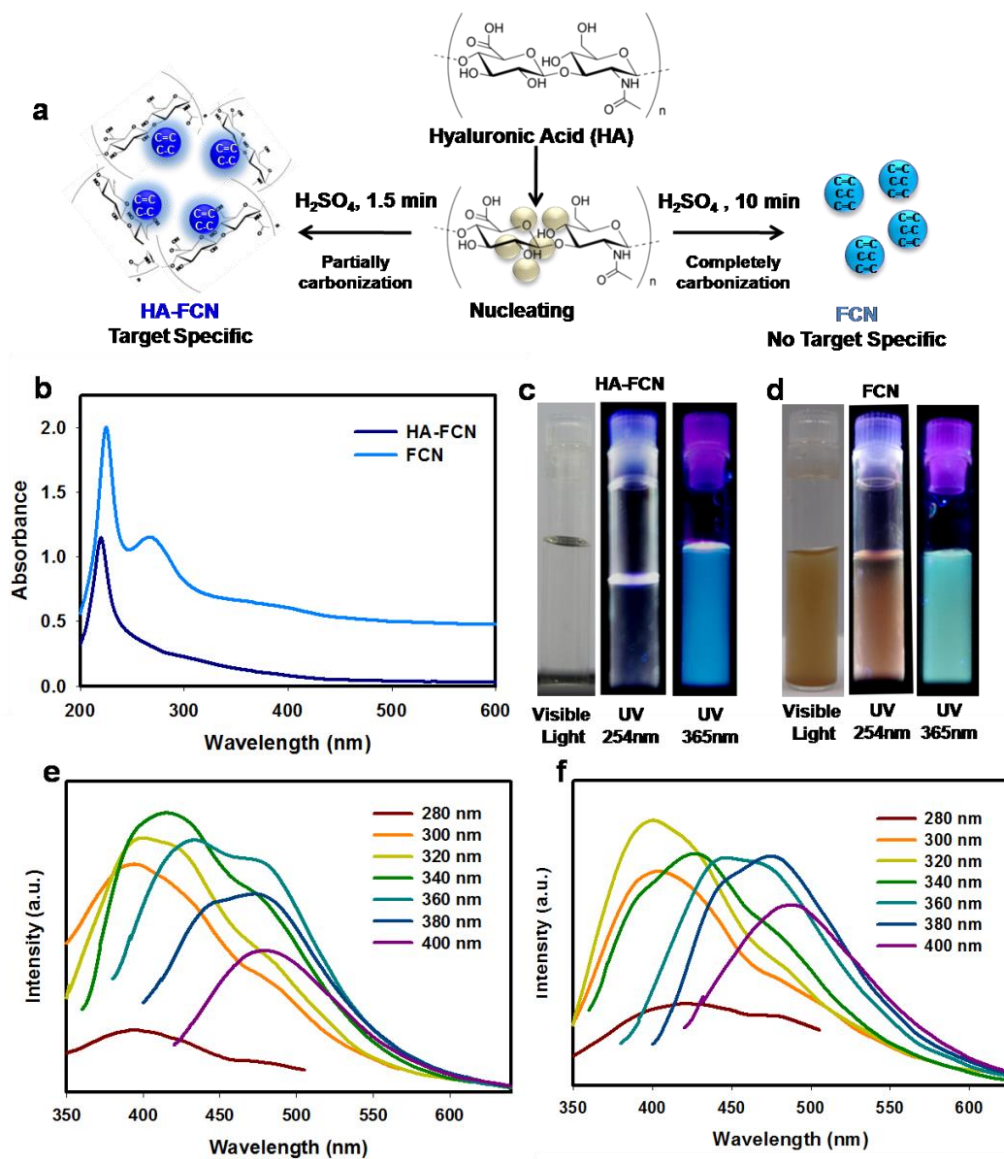
Results and Discussion

Fig. 1 Scheme of HA-FCN and FCN preparation from hyaluronic acid (a). UV-vis absorption spectra of the HA-FCN and FCN produced
5 (b). An illuminated photograph of aqueous solutions (1 mg mL^{-1}) of HA-FCN (c) and FCN (d) under visible light, and 254 nm and 365 nm UV lamps, respectively. The fluorescence emission spectra of HA-FCN (e) and FCN (f) at different excitation wave lengths (280-400 nm).

Target bio-imaging and delivery are promising new approaches
10 for the study and treatment of a variety of diseases, including, most notably, cancer.[16, 17] Depending on the dehydration method, our reported HA-FCN (partial carbonized FCN) and FCN (completed carbonized FCN) are capable of performing target delivery, as well as fluorescence bioimaging. The carbonization
15 process increased with increasing dehydration time however emission wavelength remains unchanged after 5 min. The proposed chemical structure is schematically shown in Fig. 1a.[17]

To understand the capability of multicolor fluorescence emission,
20 the prepared HA-FCN and FCN were excited at different wave lengths, and the spectral intensity was recorded.[10] Fig. 1 (e and f)

shows emission fluorescence spectra of HA-FCN and FCN, respectively. The HA-FCN presented a maximum emission at an excitation wavelength of 340 to 360 nm, whereas FCN showed
25 maximum emission in the 320 to 380 nm range. The UV-vis absorption of HA-FCN exhibited an intense peak at 220 nm, which was identified as the degraded HA fragment and the presence of a converted double bond,[18] whereas FCN showed two peaks centered at about 230 nm and 265 nm, respectively (Fig.
30 1b). The shift in the peak from 220 to 230 nm with an additional absorption band at 265 nm depicted an increased level of carbonization after breakdown of the main chain by strong dehydrating agents.[19, 20] Furthermore, compared with HA-FCN, complete carbonized FCN showed a decreased intensity with a

red shift in the emission spectrum, and fluorescence emission wavelength did not changed with concentration (Fig. S1). [20] With illumination from a lamp at 365 nm, HA-FCN strongly emitted a blue color (Fig. 1c), while FCN emitted a distinguished greenish-blue color (Fig. 1d). The quantum yield (%) of HA-FCN and FCN showed 1.9 and 1.3, respectively. At the same time fluorescence lifetime of HA-FCN and FCN measured in 375 nm wavelength shows 9.7 ns and 5.65 ns, respectively (Fig. S2). [13] These values are comparable to those of FCN which is derived from carbon sources. [12, 13] These results therefore demonstrated excitation-dependent emission spectra with identical photo physical properties, having the capacity to be utilize in different fluorescence-based tool development.

Fig. 2 Transmission Electron Microscope (TEM) images of HA-FCN and FCN, showing size and shape (a). The scale bar is 10 nm. HRTEM images of HA-FCN and FCN (b). The scale bar is 5 nm. Dynamic Light Scattering (DLS) measurements indicating the size distribution of HA-CFN and FCN (c). The GPC retention times for HA-FCN and FCN, respectively (d). ^{1}H NMR spectra of HA-FCN and FCN, respectively (e). The indicated peaks, (1), (2),

(3) and (4), represent the corresponding protons that are an integral part of hyaluronic acid. The asterisks show the residual peak of the solvent.

The size and shape of nanoparticles with arrangement of constituent atoms directed the predictable energy transfer, exhibiting stability with efficient fluorescence emission. In contrast to molecular probes, each nanoparticle probe is believed to have variance in size or molecular diameter. [21, 22] The variation in orientation, exhibiting size-dependent properties, allowed for differences in the fluorescence emission levels. The TEM image (Fig. 2a) showed that HA-FCN had a size less than 20 nm, while a comparatively smaller size was observed for FCN. Fig. 2b shows the high resolution TEM (HRTEM) image and lattice distance of a small area near the particle center. The lattice d-spacing of HA-FCN (0.353 nm) shows almost similar to graphene like particles and comparative small lattice spacing identified from the FCN (0.246 nm) attributable to diamond-like carbon, suggesting internalized carbon particles during dehydration process. [21] The morphological shape of both HA-FCN and FCN was further examined through AFM analysis. HA-FCN was observed to have a depth of about 2.5 nm, whereas FCN showed a slightly smaller diameter (2 nm) depth between the surface and particle (Fig. S3). The comparative size difference between HA-FCN and FCN is likely the reason for the different fluorescence emissions with red shift by sp2 carbon amounts into the fluorescence nanoparticles above 300 nm excitation wavelength. In hydrodynamic size distribution, the dynamic light scattering (DLS) showed the particle size distribution of HA-FCN in between 27-30 nm and average to be 28.5 nm, whereas FCN was within 11-14 nm limits and average size 12 nm diameter (Fig. 2c) shows almost similar trends as obtained by the TEM. Meanwhile, the retention time of GPC trace showed two ranges of molecular weight for HA-FCN: (Mn) 1.20 and 520 kDa, whereas FCN represented a uniform size of 1.21 kDa (Fig. 2d). These were nearly fair size distributions, where the particle size and morphological structures implied promising applicable potentiality. [10] Specifically, the uniform size distribution appeared advantage of predetermined biodistribution, and spherical morphological shape promised for convenient surface functionalization with target compound and biological species for biological application. [10] The structural compositions of HA-FCN and FCN were confirmed by their ^{1}H NMR spectra. The characteristic proton peaks of HA-FCN at 1.9 ppm [3H, -NH-CO-CH_3], 3.6-3.7 ppm [2H, -CH_2-OH] and 4.2-4.3 ppm [1H, -CH-] supported the identical ^{1}H NMR for HA (Fig. 2e). [23] However, these respective peaks were found to be absent in FCN, that was also derived from same source material, HA (Figure 2e). Fig. S5 shows the FT-IR of HA-FCN and FCN, where the peaks at 3640, 3400, 1656, 1320 and 1250 cm^{-1} clearly demonstrated the presence of O-H stretching of a free hydroxyl group, an H-bonded hydroxyl group, a C=O stretch for carboxylic acids, a C-O stretch for carbonyl groups, and a C-N stretch for aliphatic amines, respectively. [24, 25] The results of zeta potential measurements provided further evidence to support this analysis. HA-FCN and FCN both showed a highly negative charge (-mV) irrespective to the pH (ranged from 5.0 to 8.5), suggesting that the surfaces of HA-FCN and FCN were negatively charged due to
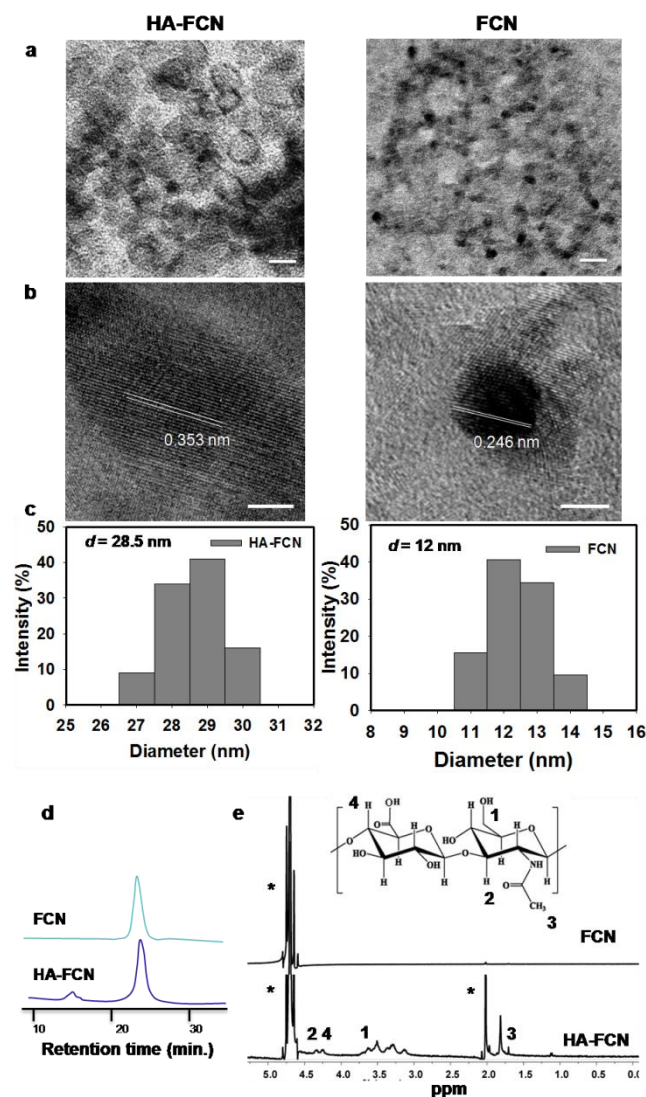
carboxyl groups (Fig. S6). However, the zeta potential of HA-FCN was slightly lower, due to the prominent role of amino groups allowing depression effects of the carboxylic groups (Fig. S7).[26, 27] Therefore, in a given wavelength, the difference in structural constituents facilitated the difference in the level of energy transfer which was previously observed under a UV lamp (Fig. 1c and 1d) for HA-FCN and FCN.
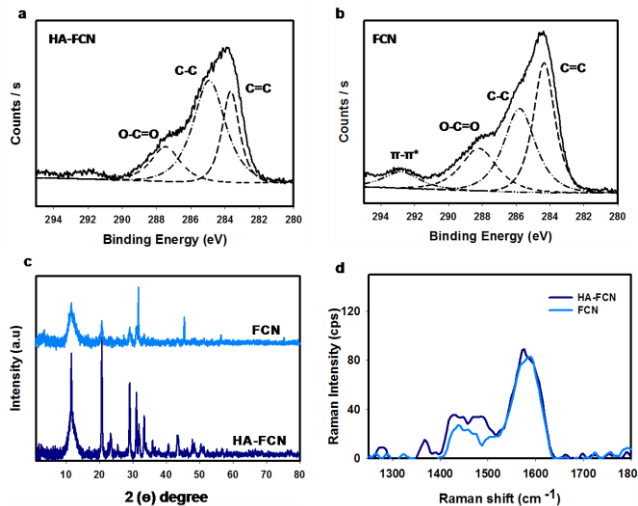

Fig. 3 X-ray photoelectron spectroscopy (XPS) spectra of C1s peaks of HA-FCN (a) and FCN (b). The X-ray diffraction (XRD) patterns in the 2θ range 1-80° of HA-FCN and FCN (c). Raman shift (cm^{-1}) of G/D bands of the HA-FCN and FCN, respectively (d).

The elemental composition was identified through X-ray photo electron spectroscopy (XPS) analysis (Fig. 3a and 3b). The specified XPS C1s spectrum demonstrated the presence of three identical peaks of C=C, C-C, and O-C=O at around 284, 285.72 and 288 eV in both HA-FCN and FCN,[28] whereas the percentage ratio of sp^2 type carbon significantly increased in the case of FCN (Table S1). Finally, a prominent π-π* transition peak appeared at 292 eV, depicting the presence of some carboxylic and hydroxyl groups on the carbonized FCN.[29] The total elemental area of the HA-FCN shows 17.22 % carbon, 0.60 % nitrogen and 82.18 % oxygen, where the FCN contents 38.6 % carbon, 5.4 % nitrogen and 56 % oxygen, respectively. The complete carbonization of FCN represents increased elemental content of carbon compare to HA-FCN (Table S1). However the HA-FCN shows increased elemental content of oxygen due to large number of carboxyl groups obtained by carbonization process under aqueous condition.[29] The elemental analysis data shows the almost same trends as obtained by the XPS (Table S1). The powder can be thought of as a collection of thousands of vary small crystals with different orientation. The X-ray diffraction (XRD) patterns of both HA-FCN and FCN showed well-resolved diffractions, appearing at 2θ = 10, 21, 29 and 32, but a very weak multi peak was observed later from HA-FCN (Fig. 3c). The identified common peaks (10 ∼ 30°) between HA-FCN and FCN reflected the amorphous nature of the carbonized particles,[30] whereas the weak diffraction after 32° (2θ) in HA-FCN depicted the incomplete carbonization approach, allowing the carbon sheet to

be oriented in a random fashion, while the complete carbonization of FCN showed a nearly homogeneous pattern.[31] An apparent G band at 1590 cm^{-1} and a D band at 1360 cm^{-1} were observed in the Raman spectrum of both HA-FCN and FCN (Fig. 3d), implying sp^2 with sp^3 hybrid carbons on these nanoparticles. The intensity ratio [I$_D$/I$_G$], which is often used to correlate the structural constitute of carbonized nanoparticles, also indicated different ratios of the sp^2/sp^3 form of carbon. Therefore, we concluded from the intensity of the D/G bands that HA derived HA-FCN was mainly composed of sp^3 carbons, whereas FCN had a decreased level of sp^3 carbons.[32, 33] The carbonized materials usually containing a mixture of sp2 type π (pi) bonding, and the light emission from such carbon systems is a consequence of geminate recombination of localized e-h (electron-hole) pairs in sp2 clusters, which essentially behave as the luminescence centers or chromophores. Though the emission energy bandgap depends on the size, shape, and fraction of the sp2 domains, tunable light emission can be achieved by controlling the nature of carbonization.[22]

To estimate the possible cytotoxic effects on living samples, the MTT assay for HA-FCN and FCN was carried out on MDCK, MDAMB and A549 cells. Cell viability of nearly 100% was found for up to 1 mg mL^{-1} concentrations on each type of cells for both HA-FCN and FCN (Fig. S8). This concentration-independent cells viability demonstrated the substantial biocompatibility and minimum cytotoxicity of both of the prepared nanoparticles (HA-FCN/FCN).
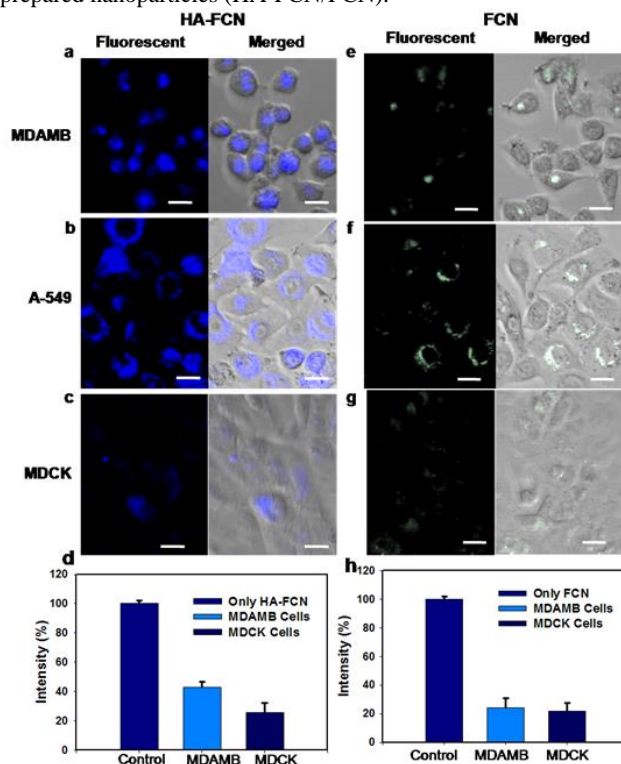

Fig. 4 Confocal microscope images of MDAMB (a and e), A549 (b and f) and MDCK (c and g) cells treated with HA-FCN or FCN at 0.01 mg mL^{-1} concentrations. All scale bars indicate 20 μm. The quantitative cellular accumulation of d) HA-FCN and h) FCN in MDAMB and MDCK cells after incubation for 4 h.

Visualization of the fluorescence level in cells allows evaluation of the cellular interactions for advance biomedical applications.[34, 35] To evaluate cellular uptake of both HA-FCN and FCN, the uptakes were examined for normal MDCK cells and cancerous MDAMB and A-549 cells. All of the cell samples were fixed for a predetermined period of time with culture medium containing HA-FCN and FCN, and the cells were then examined using confocal microscope. As shown in Fig. 4 (a, b and c), stronger fluorescence signals were detected from MDAMB and A-549 cells than in the normal MDCK cells. This may be due to the over expression of CD44 receptor on the surface of the MDAMB and A-549 cells, which facilitates efficient uptake of the remaining HA particles of HA-FCN.[36] The content of the HA retains about 18 % which is decorated on the surface of HA-FCN measured by XPS and TGA (Table S1, Fig. S9). The FCN treated *in vitro* study demonstrated fluorescence emission independent of the cell type, which was confirmed through fluorescent color observation (Fig. 4e, 4f and 4g). The characteristic less densely packed of MDAMB cells suggesting localization of HA-FCN/ FCN in nuclear membrane where A549 cells exhibit reduce endocytotic pathway retaining cytoplasmic organelles.[36] To evaluate the quantitative cellular accumulation, the MDAMB and MDCK cells were again treated with HA-FCN and FCN for 4h at 0.5 mg mL^{-1} concentrations. Both types of HA-FCN-treated cells showed a considerable difference in intensity of fluorescence, with a 41 % intensity exhibited by MDAMB and a 25 % intensity by MDCK cells (Fig. 4d). Both kinds of FCN-treated cells showed almost similar intensity (about 21-22 %). The larger amount of HA-FCN taken up by the MDAMB cancer cells clearly demonstrated target selectively *via* receptor-mediated endocytosis, whereas the cell-type independent FCN accumulation indicated size-dependent particle permeability (Fig. 4h).[37] Moreover, the enhanced permeability and retention effect (EPR) might also play a vital role for accumulating large numbers of nano-sized particles inside tumor.
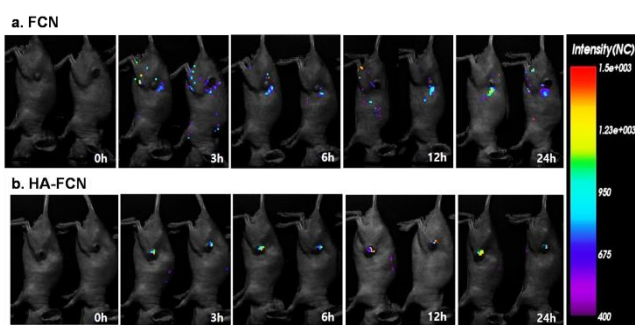

Fig. 5 *In vivo* biodistribution and corresponding intensities of FCN (a) and HA-FCN (b) of tumor-bearing nude nice at 0 h, 3 h, 6 h, 12 h and 24h time interval.

After injecting FCN and HA-FCN (30 mg/mL) through tail vein, we observed gradually increasing fluorescence signals at tumor site in flank tumor model in accordance with fast cellular uptake in tumor cells. From 3 h post-injection of HA-FCN (Fig. 5b), strong fluorescence signals were observed at the tumor site. However FCN (Fig. 5a) shows bright fluorescence signals throughout the whole mice body showing their long circulation. At 24h post-injection, tumor sites in those mice were significantly delineated from the surrounding normal tissues, proving the tumor-specific targeting of HA-FCN.
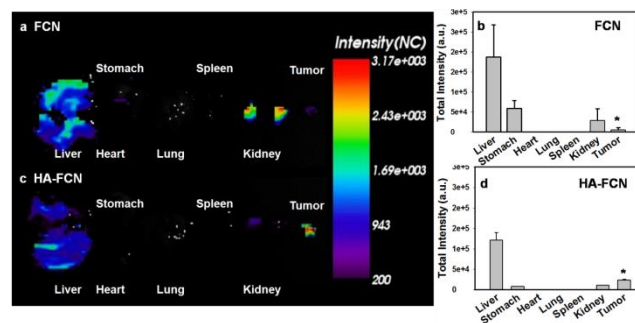

Fig. 6 The *ex vivo* biodistribution and corresponding intensities of FCN (a and b) and HA-FCN (c and d), respectively, from liver, heart, lung, spleen, kidney and tumor after dissection, with the normalized intensity from dissected organs (n=3).

In *ex vivo* fluorescence images of excised organs (liver, kidney, heart, lung, spleen, and tumors) at this time point, the highest intensity was observed in the tumor tissue (Fig. 6c and 6d). The histological fluorescence image of the excised flank tumor tissue revealed red spots of HA-FCN which were localized in the tumor tissue, not in the normal skin tissue. Furthermore, the total photon counts per gram of excised tumor tissues were substantially higher than those from the other organs (Fig. 6c and 6d).[38] The fluorescence images and intensity graph obtained from the tumor-bearing mice after injection of particles also demonstrated the circulation time of HA-FCN to be much longer than FCN. In the case of FCN, adjusted to similar fluorescence intensity, most of the particles were accumulated mainly in the liver, kidney from the initial time, while the fluorescence intensity in tumor was much lower than in the liver tissue (Fig. 6a and 6b). The overall *ex vivo* biodistribution suggested that the HA-FCN accumulated into the tumor site 2-3 times more compare with FCN.

Conclusions

In conclusion, the biocompatible HA was used for the first time as a fluorescence materials source. Due to the huge demand of biocompatible target delivery and imaging probes, we can synthesize fluorescent nanoparticles, as well as fluorescent emission having unusual target efficiency. The remaining HA parts in HA-FCN via carbonization process were selective to simultaneously deliver the target molecules and for imaging applications. TEM images confirmed the size of both HA-FCN and FCN, which facilitated their ability for *in vitro* cellular uptake and *in vivo* biodistribution, with safe clearance after administration. The size distribution in aqueous medium (DLS measurement) and colloidal stability from elevated zeta potential charge were also promising for chemical stability. Moreover, ^{1}H NMR, FT-IR, XPS, and XRD characterized the chemical groups to have semi/nano crystalline carbonized properties, which would be flexible for easy fabrication with other carriers. We also expect the enormous potential for future use of HA-FCN and FCN in

bioimaging, drug delivery, bio-sensors, diagnostic and biomedical fields.

Acknowledgements

Notes and references

a Department of Chemistry, Korea Advanced Institute of Science and Technology (KAIST), Daejeon 305-701, Republic of Korea.
b Department of Chemical and Biological Engineering, Korea National University of Transportation, Chungju 380-702, Republic of Korea.
c School of Pharmacy, Sungkyunkwan University, 300 Cheoncheon-dong, Jangan-gu, Suwon, Gyeonggi-do 440-746, Republic of Korea
d Department of Polymer Science and Engineering, Korea National University of Transportation, Chungju 380-702, Republic of Korea.
e Department of IT Convergence, Korea National University of Transportation, Chungju 380-702, Republic of Korea.
f Department of Otolaryngology-Head and Neck Surgery, College of Medicine, Kosin University, Busan, Republic of Korea.

DOI: 10.1039/b000000x/

1   M. J. Ruedas-Rama, J. D. Walters, A. Orte, E. A. H. Hall, *Analytica Chemica Acta*, 2012, **751**, 1.
2   S. Mitragotri, J. Lahann, *Nat Mater*, 2009, **8**, 15.
3   B. Toole, Hyaluronan, *Nature Reviews Cancer*, 2004, **4**, 528.
4   M. Khanmohammadi, A. B. Khoshfetrat, S. Eskandamezhad, N. F. Sani, S. Ebrahimi, *J. Ind. Eng. Chem.*, 2014, **20**, 4371.
5   M. K. Cowman, S. Matsuoka, Carbohydrate research, 2005, **340**, 791.
6   O. P. Varghese, W. Sun, J. Hilbom, D. A. Ossipov, *J. Am. Chem. Soc*, 2009, **131**, 8781.
7   D. Libe, C. P. Richter, C. Drees, O. Birkholz, C. You, E. Rampazzo, *Nano. Lett.*, 2014, **4**, 2189.
8   H. S. Choi, W. Liu, P. Misra, E. Tanaka, J. P. Zimmer, B. I. Ipe, *Nature Biotechnology*, 2007, **25**, 1165.
9   S. M. Hussain, K. L. Hess, J. M. Gearhart, K. T. Geiss, J. J. Schlager, *Toxicology in Vitro*, 2005, **19**, 975.
10   S. N. Baker, G. A. Baker, *Angew. Chem. Int. Ed*, 2010, **49**, 6726; S. Zhu, Q. Meng, L. Wang, J. Zhang, Y. Song, H. Jin, K. Zhang, H. Sun, H. Wang, and B. Yang, *Angew. Chem. Int. Ed.*, 2013, **52**, 3953.
11   J. K. Jaiswal, H. Mattoussi, J. M. Mauro, S. M. Simon, *Nature Biotechnology*, 2002, **21**, 47.
12   H. Liu, T. Ye, C. Mao, *Angew. Chem. Int. Ed*, 2007, **46**, 6473; S. O. Jeon, J. Y. Lee, *J. Ind. Eng. Chem.*, 2011, **17**, 105.
13   A. T. R. Wiliams, S. A. Winfield, J. N. Miller, *Analyst*, 1983, **108**, 1067; Z. L. Wu, P. Zhang, M. X. Gao, C. F. Liu, W. Wang, F. Leng, C. Z. Huang, *J. Mater. Chem. B*, 2013, **1**, 2868.
14   J. Jeong, A. K. Roy, S. H. Kim, J. E. Lee, J. H. Jeong, I. In, & S. Y. Park, *Nanoscale*, 2014, **6**, 15196.
15   A. A. Nahain, J. E. Lee, I. In, H. Lee, K. D. Lee, J. H. Jeong, *Mol. Pharmaceutics*, 2013, **10**, 3736.
16   M. Kamat, K. El-Boubbou, D. C. Zhu, T. Lansdell, X. Lu, W. Li, *Bioconjugate Chem*, 2010, **6**, 2336.
17   C. Minelli, S. B. Lowe, M. M. Stevens, *Small*, 2010, **21**, 2128; H. Li, Z. Kang, Y. Liu, S.T. Lee, *J. Mater. Chem.*, 2012, **22**, 24230; S. Zhu, Y. Song, X. Zhao, J. Shao, J. Zhang, B. Yang, *Nano Research*, **2014**, DOI: 10.1007/s12274-014-0644-3.
18   W. M. Tian, C. L. Zhang, S. P. Hou, X. Yu, F. Z. Cui, Q. Y. Xu, *J. Control. Release*, 2005, **102**, 13.
19   J. A. Alkrad, Y. Mrestani, D. Stroehl, S. Wartewig, R. Neubert, *J. Pharm, Biomed. Anal*, 2003, **31**, 545.
20   J. K. Kim, P, Srinivasan, J. H. Kim, J. Choi, H. J. Park, M. W. Byun, *Food Chemistry*, 2008, **109**, 763.
21   K. Lee, V. P. Drachev, J. Irudayaraj, *ACS Nano*, 2011, **5**, 2109; C. Shen, Y. Sun, J. Wang and Y. Lu, *Nanoscale*, 2014, **6**, 9139; Z. Su, W. Zhou, Y. Zhang, *Chem. Commun.*, 2011, **47**, 4700; L. Tian, D. Ghosh, W. Chen, S. Pradhan, X. Chang, S. Chen, *Chem. Mater.*, 2009, **21**, 2803.
22   G. Eda, Y. Y. Lin, C. Mattevi, H. Yamaguchi, H. A. Chen, I. S. Chen, C. W. Chen, and M. Chhowalla, *Adv. Mater.*, 2010, **22**, 505; S. M. Sharker, C. J. Jeong, S. M. Kim. J. E. Lee, J. H. Jeong, I. In, S. Y. Park, *Chem. Asian. J*, 2014, **9**, 2921.
23   G. Saravanakumar, K. Y. Choi, H. Y. Yoon, K, Kim, J. H. Park, I. C. Kwon, *Int. J. Pharm*, 2010, **394**, 154.
24   D. Osswald, M. Havel, Y. Gogotsi, *J. Raman Spectrosc*, 2007, **38**, 728.
25   N. Vigeshwaran, N. M.Ashtaputre, P. V. Varadarajan, R. P. Nachane, K. M. Paralikar, R. H. Balasubramanya, *Mater. Letter.*, 2007, **61**, 1413.
26   S. Chandra, P. Das, S. Bag, D. Laha, P. Pramanik, *Nanoscale*, 2011, **3**, 1533.
27   K. Y. Suh, J. M. Yang, A. Khademhosseini, D. Berry, T. T. Tran, H. Park, *J. Biomed. Mater. Tes. B. Appl. Biomater*, 2005, **72**, 292.
28   Y. Toda, H. Hirayama, N. Kuganathan, A. Torrisi, P. V. Sushko, H. Hosono, *Nature Communication 4*, 2013, **2378**, 1.
29   V. Datsyuk, M. Kalyva, K. Papagelis, J. Parthenios, D. Tasis, A. Silkou, *Carbon*, 2008, **46**, 833; J. Zhou, Z. Sheng, H. Han, M. Zou, C. Li, *Materials Letters*, 2012, **66**, 222; B. De, N. Karak, *Rsc Advances*, 2013, **3**, 8286.
30   I. Moriguchi, R. Hidaka, H. Yamada, T. Kudo, H. Murakami, N. Nakashima, *Adv. Mater.*, 2006, **18**, 69.
31   M. Hara, T. Yoshida, A. Takagaki, T. Takata, J. N. Kondo, S. Hayashi, *Carbon*, 2012, **50**, 1298.
32   A. Rahy, C. Zhou, J. Zheng, S. Y. Park, M. J. Kim, I. Jang, *Carbon*, 2012, **50**, 1298.
33   J. Hodkiewitz, Thermo Scientific, *Application note*, 51901.
34   M. D. Massich, D. A. Giljohann, A. L. Schmucker, P. C. Patel, C. A. Mirkin, *ACS Nano*, 2010, **4**, 5641.
35   X. Chen, Y. Yan, M. Mullner, M. P. Koeverden, K. Noi, W, Zhu, *Langmuir*, 2004, **30**, 2921.
36   N. Doshi, A. J. Swiston, J. B. Gilbert, M. L. Alcaraz, R. E. Cohen, M. F. Rubner, *Adv. Mater.*, 2011, **23**, H105; J. A Coulter, S. Jain, K. T Butterworth, L. E Taggart, G. R Dickson, S. J McMahon, W. B Hyland, M. F Muir, C. Trainor, A. R Hounsell, J. M O'Sullivan, G. Schettino, F. J Currell, D. G Hirst, K. M Prise, *International Journal of Nanomedicine*, 2012, **7**, 2673.
37   E. Gullotti, Y. Yeo, *J. Control. Telease*, 2012, **164**, 170.
38   H. Y. Yoon, H. Koo, K. Y. Choi, S. J. Lee, K. Kim, I. C. Kwon, *Biomaterials*, 2012, **33**, 3980; L.Yang, Y. C. Lee, M. I. Kim, H. G. Park, Y. S. Huh, Y. Shao, H. K. Han, *J. Mater. Chem. B*, 2014, **2**, 7567.

Nanoscale Accepted Manuscript